


## Article

# Dynamic and Energy Consumption Characteristics of Sandstone Ring Specimens under Dry and Wet Cycling

Qi Ping <sup>1,2,\*</sup> , Shiwei Wu <sup>1,2</sup>, Xiangyang Li <sup>1,2</sup>, Yijie Xu <sup>1,2</sup>, Jing Hu <sup>1,2</sup> and Shijia Sun <sup>1,2</sup>

<sup>1</sup> State Key Laboratory of Mining Response and Disaster Prevention and Control in Deep Coal Mine, Anhui University of Science and Technology, Huainan 232001, China; 2021200374@aust.edu.cn (S.W.); 2021200370@aust.edu.cn (X.L.); 2021200476@aust.edu.cn (Y.X.); 2021200474@aust.edu.cn (J.H.); 2021200516@aust.edu.cn (S.S.)

<sup>2</sup> School of Civil Engineering and Architecture, Anhui University of Science and Technology, Huainan 232001, China

\* Correspondence: ahpinqi@163.com; Tel.: +86-139-5645-9398

**Abstract:** The aim of this study was to examine the effects of sandstone ring specimens with different inner diameters on dynamic compression mechanical characteristics after dry and wet circulation. To carry out our study, we subjected a sandstone ring specimen with a 50 mm outer diameter and a 0~25 mm inner diameter to 10 cycles of dry and wet circulation. Afterward, we recorded the specimen's basic physical parameters and used a split-Hopkinson pressure bar (SHPB) test device to perform an impact compression test. Following dry and wet circulation, our results showed that the mass loss rate increased and the volume expansion rates and density decreased with the increase in the inner diameter of the sandstone ring sample. Simultaneously, with the increase in the inner diameter of the specimen ring, the dynamic compressive strength of the specimen presented an exponential negative correlation, the dynamic elastic modulus presented a quadratic negative correlation, and the dynamic peak strain presented a quadratic positive correlation. Concurrently, the average particle size of the specimen decreased, and the degree of breakage increased with the increase in the sandstone sample's inner diameter. Regarding the energy analysis performed in this study, the sandstone ring sample's energy dissipation increased, and its kinetic performance evidently weakened with the increase in the ring sample's inner diameter. The results of this study have certain reference values for the construction and maintenance of natural cavity rock and underground hard rock roadways.

**Keywords:** rock dynamics; ring sample; dynamic compression; energy; SHPB (split-Hopkinson pressure bar)



**Citation:** Ping, Q.; Wu, S.; Li, X.; Xu, Y.; Hu, J.; Sun, S. Dynamic and Energy Consumption Characteristics of Sandstone Ring Specimens under Dry and Wet Cycling. *Appl. Sci.* **2024**, *14*, 2646. <https://doi.org/10.3390/app14062646>

Academic Editor: Tiago Miranda

Received: 22 February 2024

Revised: 18 March 2024

Accepted: 19 March 2024

Published: 21 March 2024



**Copyright:** © 2024 by the authors. Licensee MDPI, Basel, Switzerland. This article is an open access article distributed under the terms and conditions of the Creative Commons Attribution (CC BY) license (<https://creativecommons.org/licenses/by/4.0/>).

## 1. Introduction

In water storage and energy storage reservoir projects, due to seasonal water level changes, pumping energy storage, and drainage power generation, the drainage channels and natural holes in the engineering rock mass will be subjected to a dry and wet cycle environment, and the influx of water will form dynamic loads. Owing to these issues, it is of great importance to study rock samples with different inner diameters after they are subjected to dry and wet cycles for excavation and maintenance in underground engineering. To this end, we specifically collated the relevant studies of many scholars on the effects of wet and dry cycles and ring rock specimens on rock dynamics.

In the application of split-Hopkinson pressure bar (SHPB) technology, Ping et al. [1] carried out SHPB impact compression tests on limestone specimens following high-temperature cycle treatment at room temperature (25 °C) and 100 °C~1000 °C. Mahabadi et al. [2] proved the feasibility of the finite-discrete element method to simulate the dynamic response of rock by using an SHPB test device in their study. Meng et al. [3] carried out an SHPB impact compression test on reef limestone and analyzed the difference in dynamic mechanical

properties between reef limestone and common rocks. Deshpande et al. [4] found that for an SHPB test carried out on large-diameter samples, the choice of a pulse shaper with a diameter of 15–20 mm and a width of 2.5 mm would be more conducive to the smooth dynamic force of rock samples. Zheng et al. [5] used an SHPB to study the dynamic mechanical properties of sandstone under impact loads. Sunita et al. [6] used the SHPB test apparatus to measure the dynamic properties of various rocks at high strain rates. Wen et al. [7] used an SHPB test device to explore the effect of bedding dip angle on the mechanical properties of and damage to composite rock mass. Fakhimi et al. [8] studied the mechanical properties of sandstone under uniaxial compression load by using the splitting SHPB test and modeling. Yue et al. [9] verified a new calculation method for examining the dynamic splitting tensile strain rate of an SHPB through numerical calculations and experiments. Demirdag et al. [10] studied the effect of porosity and density on the dynamic mechanics of carbonate rocks by using the SHPB test apparatus.

Ke et al. [11], in their research on rock subjected to wet–dry cycles or annular rock samples, used computed tomography, electron microscopy, and pore and crack analysis systems to study the microscopic changes of sandstone under the aforementioned wet and dry cycles. Tan et al. [12] explored the damage process of red sandstone under the coupled action of dry and wet cycling and fatigue load from three aspects: deformation, energy, and damage, and explored the crack change rule of the sample. Chai et al. [13] carried out static uniaxial tests and impact compression tests on rocks subjected to different dry and wet cycles to reveal the effects of these cycles on the dynamic and static mechanical properties of rocks with filled joints. Wang et al. [14] used acoustic emission (AE) to detect the effects of wet and dry cycles on damage to argillaceous sandstone. Wei et al. [15] carried out shear creep tests on gray shale after dry and wet cycles and analyzed the influence of the number of cycles on creep strain and cumulative creep strain. Li et al. [16] used a direct shear test and established a damage and deterioration model to analyze the deterioration rule of mica quartz schist caused by dry and wet cycles. Zhu et al. [17] revealed the influence of dry and wet cycling on the rock on a reservoir bank slope from three aspects: dynamic performance, energy dissipation rule, and crushing form, through the use of an SHPB test device. Liu et al. [18] used the MTS815 rock mechanics test system to study carbon shales with different fracture angles after dry–wet cycles to reveal the changes in strength and energy. Wen et al. [19] conducted triaxial compression tests on rocks in a reservoir area and found that dry and wet cycling reduced the peak stress, residual stress, and elastic modulus of their specimens. Li et al. [20] studied the static splitting mechanics of marble ring samples with different inner diameters. Wen et al. [21] studied the influence of dry–wet cycling on the fracture toughness and tensile strength of sandstone, and the results showed that the deterioration in the fracture toughness of sandstone samples after dry–wet cycling was greater than their tensile strength. Wu et al. [22] carried out a Brazilian disc-splitting test on sandstone rings with different inner diameters and suggested that tensile stress could not be used as a failure index. He et al. [23] used the MTS 815 rock mechanics test system to study the mechanical rules of sandstone rings under multi-stage cyclic loads. Li et al. [24] analyzed the crack development of an eccentric ring specimen following the use of the SHPB dynamic test. Liu et al. [25] revealed the temporal and spatial evolution characteristics of microcracks in granite ring specimens through the use of a uniaxial compression test.

In summary, fruitful results have been achieved in the study of rock subjected to dry–wet cycling or ring specimens. However, there are few studies on the dynamic mechanical properties of ring specimens following dry–wet cycling. In this paper, we will present, in detail, the dynamic characteristics and energy consumption analysis of sandstone ring specimens with different inner diameters following dry–wet cycling. First, the basic physical parameters of the sandstone ring specimens were determined before and after dry and wet cycle treatment, and changes in the mass, density, and volume of the specimens were compared. Afterward, the impact compression test on sandstone rings with different inner diameters following dry and wet cycling was carried out using an

SHPB test device, and their dynamic characteristics, such as dynamic stress, dynamic strain, and elastic modulus, are discussed with respect to the inner diameter of the sandstone rings. Lastly, according to the energy change and crushing form of the sandstone ring specimen, the influence of the inner diameter of the sandstone ring specimen on the deterioration of its dynamic properties is analyzed.

## 2. Ring Specimen Processing and Its Physical Parameters

### 2.1. Preparation of the Specimen for Processing

The sandstone rock samples used in this paper were taken from the Dingji coal mine in Huainan, China. After the rock samples were transported back to our laboratory, they were cored, cut, polished, and punched. The instruments used during these processes are shown in Figure 1. The preparation of the samples complied with the test methods recommended by international rock mechanics testing and the test procedures used in Chinese rock dynamics [26,27]. The rock samples were cored, cut, polished, and drilled to form a circular specimen with a thickness of  $B = 25$  mm, an outer diameter of  $D = 50$  mm, and an inner diameter of  $d = 0$  mm (complete specimen), 5 mm, 10 mm, 15 mm, 20 mm, and 25 mm. The pore size of natural porous rock and the proportion of hard rock roadway in the entire rock in underground engineering will vary. Therefore, selecting a variety of inner diameters is more suitable for engineering practice. The processed circular specimens are shown in Figure 1.

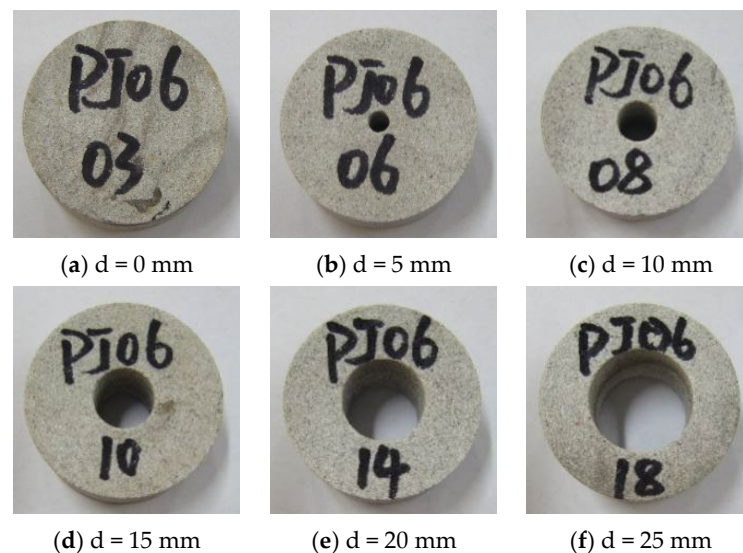


**Figure 1.** Photos of sandstone ring specimens with different inner diameters.

According to the specifications set out in [28], the sandstone ring specimens were subjected to dry–wet cycles. The specimens were placed in a sink for 48 h of natural filling. They were then taken out to wipe away any surface moisture with a dry towel, placed in an electric blast drying oven, dried at  $105$  °C for 24 h, and then cooled to room temperature naturally, with this process being defined as a dry and wet cycle.

According to relevant research results presented in another study [29], the decrease in amplitude of wave velocity and dynamic compressive strength of the coal mine sandstone specimens after eight dry–wet cycles was essentially stable. In this study, we chose ten as the number of dry–wet cycles. A sandstone ring specimen following dry–wet cycling is presented in Figure 2.

In Figure 2, it can be seen that the apparent color of the sandstone ring specimen following 10 dry–wet cycles changed to light brown, the number of fine particles on the surface of the specimen increased, and the sand's appearance was enhanced. It was preliminarily judged that the sandstone ring specimen deteriorated following dry–wet cycling.



**Figure 2.** Sample diagram after dry and wet cycling.

## 2.2. Basic Physical Properties

The size and basic physical parameters of the sandstone ring specimens in their natural state and after 10 dry–wet cycles are shown in Table 1.

**Table 1.** Basic physical parameters of the sandstone ring specimens before and after dry and wet cycling.

Inside Diameter /mm	Specimen Number	Raw State				Dry and Wet Cycle (10th Time)			
		Height /mm	Outside Diameter /mm	Inside Diameter /mm	Quality /g	Height /mm	Outside Diameter /mm	Inside Diameter /mm	Quality /g
0	PJ06-01	25.6	50.3	0.0	125.59	25.8	50.6	0.0	122.76
	PJ06-02	25.2	50.3	0.0	125.71	25.7	50.8	0.0	122.87
	PJ06-03	25.2	50.2	0.0	125.20	25.7	50.7	0.0	122.37
5	PJ06-04	25.4	50.3	5.1	125.88	25.9	50.8	5.0	123.01
	PJ06-05	25.6	50.1	5.0	123.47	26.0	50.7	4.9	120.65
	PJ06-06	25.2	50.3	5.0	123.86	25.8	50.7	4.9	121.03
10	PJ06-07	25.3	50.2	10.1	119.19	25.5	50.8	9.9	116.41
	PJ06-08	25.4	50.3	9.9	119.61	25.8	50.7	9.7	116.81
	PJ06-09	25.4	50.1	10.0	119.68	25.9	50.5	9.7	116.88
15	PJ06-10	25.7	50.3	15.1	115.62	26.2	50.7	14.8	112.83
	PJ06-11	25.7	50.2	15.1	116.42	26.2	50.5	14.7	113.62
	PJ06-12	25.1	50.3	15.0	113.65	25.5	50.7	14.7	110.90
20	PJ06-13	25.3	50.3	20.1	104.60	25.7	50.7	19.7	101.96
	PJ06-14	25.4	50.3	19.9	104.88	25.7	50.6	19.5	102.22
	PJ06-15	25.4	50.0	20.1	103.99	25.8	50.4	19.7	101.36
25	PJ06-16	25.5	50.2	25.1	95.08	25.7	50.7	24.9	92.56
	PJ06-17	25.4	50.2	25.1	94.21	25.7	50.5	24.8	91.72
	PJ06-18	25.5	50.3	25.1	94.16	25.8	50.7	24.9	91.66

It can be seen in Table 1 that the mass of the sandstone ring specimen decreased and the volume increased after 10 dry–wet cycles. The mass loss rate, volume expansion rate, and density reduction rate of the specimen changed with the change in the inner diameter, as shown in Figure 3.

It can be seen in Figure 3 that after the dry–wet circulation of the sandstone ring specimen, the mass loss rate of the specimen increased from 2.27% to 2.63% with the increase in the inner diameter of the ring specimen. The volume expansion rate of the specimen did not change considerably when the inner diameter was 0–15 mm, with it essentially measuring between 3.75% and 4.25%; when the inner diameter was 15 mm–25 mm, the volume expansion rate of the specimen showed a downward trend, and the volume expansion rate was 3.00% when the inner diameter was 25 mm. The density of the specimen showed an increasing trend with the increase in the inner diameter of the specimen, and the trend was similar to the volume expansion rate. The density reduction rate did not change considerably with the inner diameter of 0–15 mm, with it ranging from 5.95% to

6.16%. The density reduction rate decreased significantly from 6.15% to 5.47% with an inner diameter of 15 mm~25 mm.

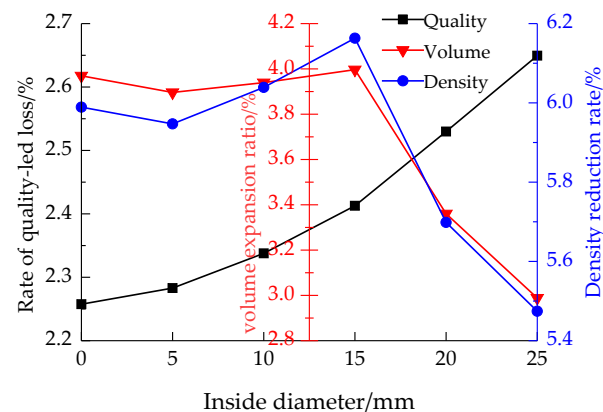


**Figure 3.** Variation in the mass, volume, and density of the sandstone ring with inner diameter.

As the inner diameter of the ring specimen increased, the wall thickness decreased, and the contact area between the specimen and water increased during the dry–wet cycle. It was found that the water in the specimen evaporated after the first dry–wet cycle. Subsequently, after the dry–wet cycle, the surface particles detached due to the increase in damage, which demonstrated that the mass loss rate of the specimen increased with the increase in the inner diameter. There were many natural cracks inside the specimen itself. During the soaking process in the wet–dry cycle, the water made the original, natural cracks inside the specimen develop and even caused the phenomenon of crack penetration, resulting in an increase in the apparent volume. During the drying process of the dry–wet cycle, the pieces of gravel found in the tiny cracks were more likely to expand and squeeze each other due to uneven stress, and then, the cracks expanded, causing an increase in the volume of the specimen. During the dry–wet cycle, the mass loss of the specimen was more obvious than the volume expansion, resulting in a downward trend in the density reduction rate.

### 3. Dynamic Performance Analysis

#### 3.1. SHPB Experiment

We used the SHPB test device (as shown in Figure 4) at the State Key Laboratory of Response and Disaster Prevention and Control in Deep Coal Mines to conduct impact compression tests on six different sandstone ring specimens with inner diameters of 0 mm, 5 mm, 10 mm, 15 mm, 20 mm, and 25 mm following ten dry–wet cycles. In the test, the impact pressure drove the bullet to impact the impact rod to produce a dynamic load. In the pre-test, the impact pressure gradually increased, and we found that the pressure could cause the sample to crack and maintain a good crushing shape according to the selection pressure of the test. Following the pre-test, 0.3 MPa was selected as the test impact pressure.



**Figure 4.** SHPB test device.

The test equipment shown in Figure 4 comprises a nitrogen tank, a transmitter, a strain gauge, and an oscilloscope. Among the equipment, the material comprising the pressure bar was high-strength alloy steel; its diameter was 50 mm; the length of the incident bar was 2 m; the length of the transmission bar was 1.5 m; the wave velocity of the pressure bar was 5380 m/s; the density was 7636 kg/m<sup>3</sup>; and the Poisson's ratio was 0.28.

The SHPB test data of the sandstone ring specimens with different inner diameters following dry–wet cycles are shown in Table 2.

**Table 2.** SHPB dynamic test data of the sandstone ring specimens.

Inside Diameter /mm	Specimen Number	Dynamic Compressive Strength /MPa	Dynamic Peak Value / $\times 10^{-3}$	Dynamic Elastic Modulus /GPa	Average Strain Rate /s <sup>-1</sup>
0	PJ06-01	94.27	2.29	42.55	172
	PJ06-02	96.34	2.27	44.49	174
	PJ06-03	93.74	2.35	45.47	176
5	PJ06-04	89.62	2.57	41.55	178
	PJ06-05	87.46	2.52	42.93	178
	PJ06-06	90.97	2.38	42.68	182
10	PJ06-07	81.30	2.79	39.74	188
	PJ06-08	79.93	2.73	38.20	185
	PJ06-09	78.58	2.80	39.42	186
15	PJ06-10	71.30	3.34	36.45	195
	PJ06-11	70.79	3.12	37.70	195
	PJ06-12	69.12	3.19	37.75	198
20	PJ06-13	65.87	3.52	31.78	202
	PJ06-14	67.53	3.87	32.84	204
	PJ06-15	65.97	3.67	31.68	205
25	PJ06-16	60.23	4.18	26.80	211
	PJ06-17	62.34	4.32	26.55	211
	PJ06-18	59.52	4.19	25.75	209

### 3.2. Dynamic Stress–Strain Curve

The typical dynamic relationships of the SHPB test following the dry and wet cycling of sandstone ring samples with different inner diameters are shown in Figure 5.

It can be seen in Figure 5 that the dynamic stress–dynamic strain curve of the sandstone ring specimen following the dry–wet cycle gradually became placid with the increase in the inner diameter, the peak point of the curve gradually moved to the lower right, and the slope of the pre-peak curve increased. With the increase in the inner diameter of the ring, the dynamic peak stress decreased and the dynamic peak strain increased.

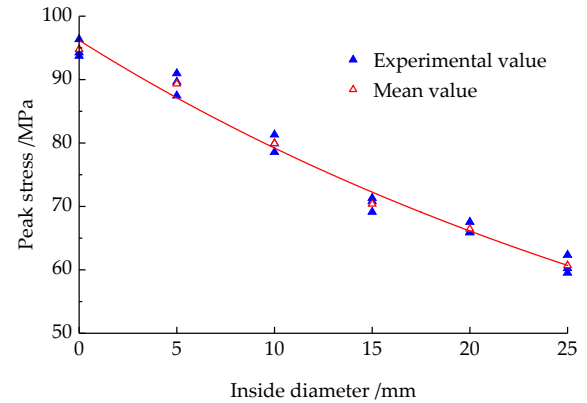
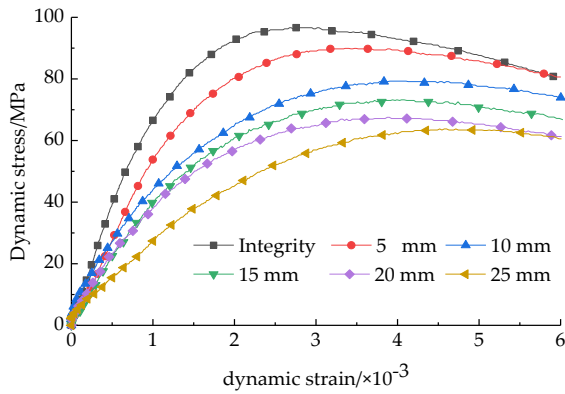
The relationship between the dynamic compressive strength of the sandstone ring specimen and its inner diameter following the dry–wet cycle is shown in Figure 5.

It can be seen in Figure 5 that the dynamic compressive strength of the sandstone ring specimen decreased gradually with the increase in its inner diameter following the dry–wet cycle. The dynamic compressive strength of the complete specimen was 94.78 MPa, which decreased to 60.70 MPa when the inner diameter was 25 mm, and the decrease was measured at 35.96%. The dynamic compressive strength had an exponential negative correlation with the inner diameter change curve, and the correlation was obvious. The fitting relationship is shown in Equation (1).

$$\sigma_0(d) = 95.7770e^{-0.0190d} \quad (R^2 = 0.9887) \quad (1)$$

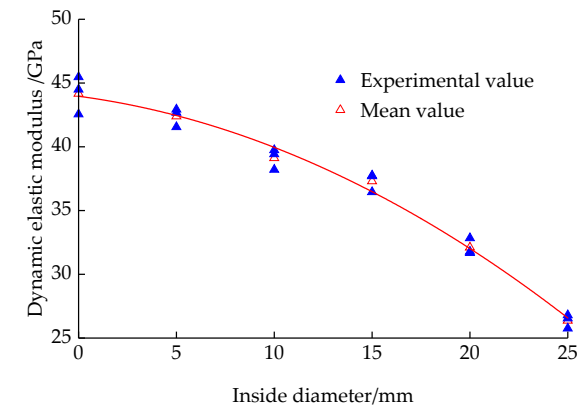
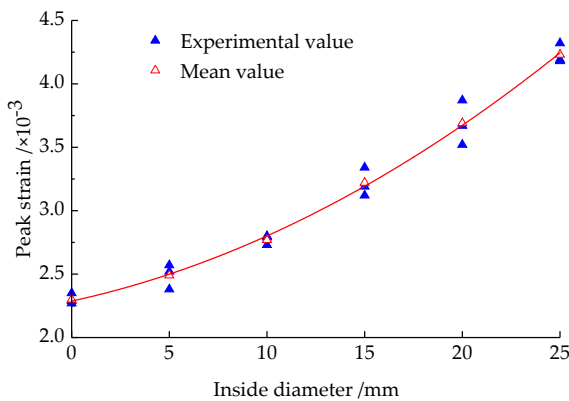
where  $\sigma_0$  is the dynamic compressive strength.

With the increase in the inner diameter of the sandstone ring specimen, the wall thickness decreased, and the effective bearing area of the specimen decreased, making this area more prone to being unstable and destroyed. At the same time, the increase in the inner diameter augments the contact surface between the specimen and the water and weakens its dynamic performance. The dry-wet cycle weakened the dynamic compressive performance of the sandstone ring, and the dynamic compressive strength decreased with the increase in the inner diameter of the specimen.



(a) Dynamic stress–strain curve of sandstone ring specimen

(b) Dynamic elastic modulus with inner diameter



(c) Dynamic elastic modulus with inner diameter

(d) Dynamic elastic modulus with inner diameter

**Figure 5.** Dynamic relationship of sandstone ring specimens with different inner diameters following dry and wet cycling.

### 3.3. Dynamic Peak Value

The variation in the dynamic peak strain of the sandstone ring specimen with the inner diameter following the dry–wet cycle is presented in Figure 5.

It can be seen in Figure 5 that the dynamic peak strain of the sandstone ring specimen increased with the increase in the inner diameter of the specimen following the dry–wet cycle. The dynamic peak strain of the complete specimen was  $2.30 \times 10^{-3}$ , and it increased to  $4.23 \times 10^{-3}$  when the inner diameter was 25 mm, which represents an increase of 83.91%. The curve of the dynamic peak strain with inner diameter was positively correlated with the quadratic function, and the correlation was significant. The fitting relationship is shown in Formula (2).

$$\varepsilon_T(d) = 2.287 + 0.033d - 0.002d^2 \quad (R^2 = 0.9991) \quad (2)$$

where  $\varepsilon_T$  is the dynamic peak strain.

As the inner diameter of the sandstone ring specimen increased, the wall thickness decreased, and the resistance to failure decreased. Simultaneously, the radial effective force area decreased and the force per unit area increased, making this area more prone to being

unstable and destroyed. Therefore, the dynamic peak strain of the specimen increased with the addition of the aperture.

### 3.4. Dynamic Elastic Modulus

Following the dry–wet cycle, the dynamic elastic modulus of the sandstone ring specimen changes with the inner diameter, as shown in Figure 5.

It can be seen in Figure 5 that the dynamic elastic modulus of the sandstone ring specimen was reduced with the increase in the inner diameter after the dry–wet cycle. The dynamic elastic modulus of the complete specimen was 44.17 GPa, and it decreased to 26.37 GPa when the inner diameter was 25 mm, which represents a decrease of 40.30%. The curve of the dynamic elastic modulus with inner diameter was negatively correlated with the quadratic function, and the correlation was significant. The fitting relationship is shown in Formula (3).

$$E = 43.9637 - 0.2046d - 0.0196d^2 \quad (R^2 = 0.9937) \quad (3)$$

where E is the dynamic elastic modulus.

During the impact compression test, the sandstone ring specimen was subjected to an axial impact load. When the specimen was complete, the axial force area was large, and the force per unit area was small. With the increase in the inner diameter of the ring specimen, the wall thickness and axial force area decreased, the force per unit area increased, and instability failure was more likely to occur. Therefore, it can be concluded that the dynamic elastic modulus of the sandstone ring specimen decreased with the increase in the inner diameter.

## 4. Analysis of Specimen Fracture Morphology and Energy Consumption

### 4.1. Analysis of Specimen Fracture Morphology

The fracture morphology of sandstone ring specimens with different inner diameters following dry–wet cycles is shown in Figure 6.

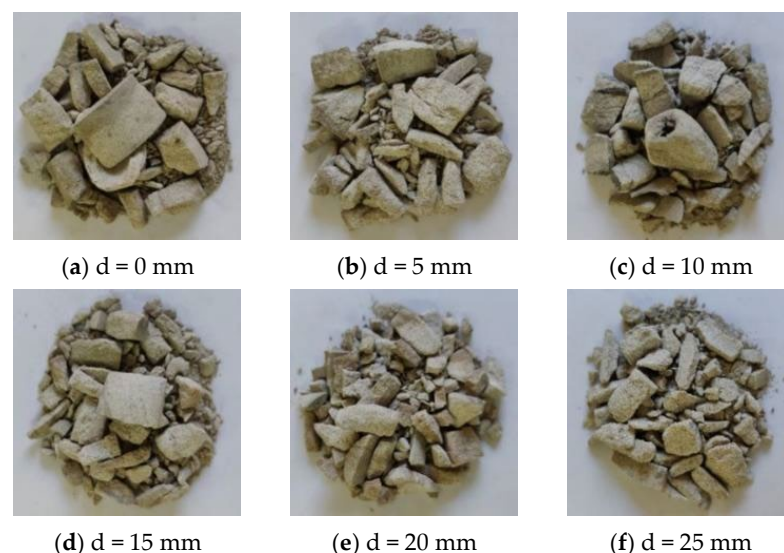


**Figure 6.** Photos showing the broken forms of the specimens.

It can be seen in Figure 6 that as the inner diameter of the sandstone ring specimen increased, the crushing shape intensified, and the fragments gradually became smaller. The degree of fragmentation was quantitatively analyzed from the perspective of average particle size. The broken average particle size formula of the specimen is shown in Formula (4).



$$d_s = \frac{\sum r_i d_i}{\sum r_i} \quad (4)$$

where  $d_s$  is the average particle size, mm;  $d_i$  is the size of the square hole sieve, mm; and  $r$  is the corresponding mass percentage of fragments.

The screening results for sandstone ring crushing specimens with different inner diameters following the dry–wet cycle are presented in Table 3, and the relationship between the average particle size of the specimen and the inner diameter size is presented in Figure 7.

**Table 3.** Impact of different inner diameter specimen fragments in terms of sieve fraction following dry and wet circulation.

Inside Diameter /mm	Size of Screen Mesh/mm									Gross Mass/g	Average Particle Size of Fragments/mm
	0	0.15	0.3	0.6	1.18	2.36	4.75	9.5	13.2		
0	2.88	3.28	5.95	4.93	5.95	7.28	18.67	21.44	52.49	122.87	8.26
5	2.08	3.56	3.15	3.74	4.80	8.44	22.11	24.82	47.95	120.65	8.16
10	2.65	2.68	3.52	7.57	3.45	5.98	21.99	23.01	45.96	116.81	7.76
15	2.77	2.91	4.23	4.56	4.85	7.75	21.71	22.88	41.17	112.83	7.26
20	2.62	4.25	4.74	6.71	4.20	8.66	16.27	18.51	35.40	101.36	6.12
25	3.57	7.70	9.71	7.28	6.67	3.74	9.04	15.64	28.37	91.72	4.81

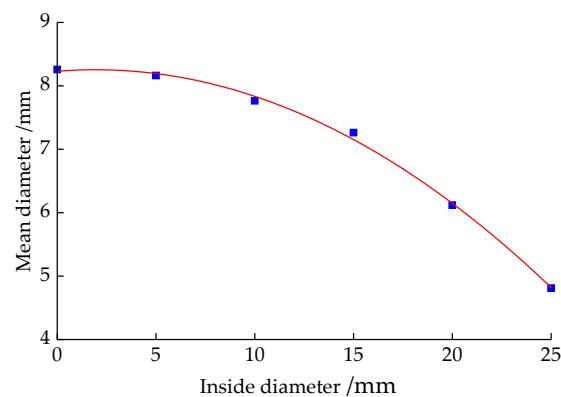


**Figure 7.** Relationship between the average particle size and the inner diameter of the specimen.

It can be seen in Figure 7 that when the inner diameter increased, the average particle size of the specimen decreased continuously, showing a quadratic function negative correlation fitting formula as shown in Formula (5).

$$d_s = 8.230 + 0.025d - 0.006d^2 \quad (R^2 = 0.9978) \quad (5)$$

The reason for the reverse growth of the average particle size and the average strain rate of the sandstone ring specimen after the dry–wet cycle may be that, under the same impact load, with the increase in the inner diameter of the specimen, the wall thickness decreased, the axial force area decreased, and the stress per unit area increased, resulting in an increase in the average strain rate. The average strain rate directly reflected the degree of deformation and fragmentation of the specimen. Therefore, it can be concluded that the degree of fragmentation increased with the increase in the inner diameter of the ring.

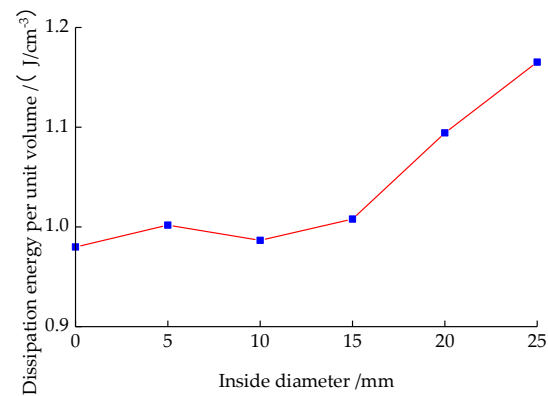
#### 4.2. Energy Consumption Analysis of Specimens

The energy change determined using the SHPB impact compression test is shown in Table 4.

**Table 4.** Energy variation in the ring sandstone specimen.

Inside Diameter /mm	Specimen Number	Incident Energy /J	Reflected Energy /J	Transmitted Energy /J	Absorbed Energy /J
0	PJ06-01	133.70	61.27	20.76	51.67
	PJ06-02	134.09	60.25	21.38	52.46
	PJ06-03	131.87	62.61	19.95	49.31
5	PJ06-04	132.96	61.57	19.59	51.80
	PJ06-05	131.82	61.09	19.27	51.46
	PJ06-06	132.18	59.41	20.46	52.31
10	PJ06-07	131.48	67.53	15.31	48.64
	PJ06-08	129.35	62.05	17.07	50.23
	PJ06-09	130.47	64.56	16.80	49.11
15	PJ06-10	131.24	69.08	12.87	49.29
	PJ06-11	128.09	67.20	11.92	48.97
	PJ06-12	127.37	69.66	10.32	46.39
20	PJ06-13	131.26	75.95	9.34	45.97
	PJ06-14	135.07	74.39	9.81	49.87
	PJ06-15	133.53	75.62	10.55	47.36
25	PJ06-16	127.17	77.22	6.30	43.65
	PJ06-17	136.77	82.81	7.88	46.08
	PJ06-18	132.52	78.56	7.62	46.34

The dissipation energy per unit volume varies with the inner diameter size, as shown in Figure 8.

**Figure 8.** Diagram of dissipated energy per unit volume with inner diameter.

From Table 4 and Figure 8, it can be seen that with the increase in the inner diameter of the sandstone ring specimen, the average absorption energy decreased, and the unit volume dissipation energy was added.

Under the impact load, the inner diameter of the sandstone ring specimen increased, the wall thickness decreased, and the volume decreased. Although the absorption energy decreased with the increase in the inner diameter, the decrease was less than the reduction in volume. Therefore, the absorption energy per unit volume increased, which directly led to an increase in the crushing degree of the specimen.

## 5. Discussion

Previous studies have shown that with an increase in the number of dry–wet cycles, the number of cracks on the specimen surface increases, and the length and width of cracks also increase [14]. Therefore, before and after the sandstone ring is subjected to dry and wet cycling, the volume of the specimen increases after the dry and wet cycle, which represents

the volume expansion of the specimen caused by the increase in the number of cracks and expansion after the dry and wet cycle. Under the action of a dynamic splitting load [22], the sandstone ring specimen will not fail with the increase in inner diameter and the decrease in wall thickness. Compared with this test, with the increase in inner diameter and the decrease in wall thickness, the sandstone ring specimen is prone to instability failure under impact compression load.

## 6. Outlook

The results of this study provide specific data support for the underground engineering of chamber types in an environment of dry and wet circulation. Simultaneously, if the axial pressure and confining pressure can be added to the environment, this will be more in line with the real engineering environment.

## 7. Conclusions

By subjecting sandstone rings with different inner diameters to the same number of dry–wet cycles, we were able to explore their basic physical parameters and dynamic properties. The main conclusions of our study are as follows:

- (1) Following the dry–wet cycle, the mass loss rate increases, the volume expansion rate increases, and the density decreases with the increase in inner diameter.
- (2) The dynamic compressive strength, peak strain, and elastic modulus are negatively correlated with the exponential function as the inner diameter increases following the dry–wet cycle.
- (3) From the perspective of broken particle size, the average particle size decreases with the increase in the inner diameter of the sandstone ring specimen, and the degree of breakage increases.
- (4) After the dry–wet cycle, the absorbed energy decreases with the increase in inner diameter, the dissipated energy per unit volume increases, and the dynamic performance weakens.

**Author Contributions:** Conceptualization, S.S.; data curation, S.W.; funding acquisition, Q.P.; methodology, Q.P.; software, S.W.; supervision, X.L., Y.X., J.H. and S.S.; validation, X.L.; visualization, Y.X. and J.H.; writing—original draft preparation, Q.P. and S.W. All authors have read and agreed to the published version of the manuscript.

**Funding:** This research was funded by the National Natural Science Foundation of China (No. 52074005, No. 52074006), the Anhui Provincial Natural Science Foundation (No. 1808085ME134), and the Anhui Postdoctoral Science Foundation (No. 2015B058).

**Institutional Review Board Statement:** Not applicable.

**Informed Consent Statement:** Not applicable.

**Data Availability Statement:** The data used to support the findings of this study are available from the corresponding author upon request.

**Acknowledgments:** Thanks to the State Key Laboratory of Mine Response and Disaster, Anhui University of Science and Technology provides experimental conditions.

**Conflicts of Interest:** The authors declare no conflicts of interest.

## References

1. Ping, Q.; Su, H.P.; Ma, D.D.; Zhang, H.; Zhang, C.L. Experimental study on physical and dynamic properties of limestone subjected to different high temperatures. *Rock Soil Mech.* **2021**, *42*, 932–942+953. [[CrossRef](#)]
2. Mahabadi, K.O.; Cottrell, E.B.; Grasselli, G. An Example of Realistic Modelling of Rock Dynamics Problems: FEM/DEM Simulation of Dynamic Brazilian Test on Barre Granite. *Rock Mech. Rock Eng.* **2010**, *43*, 707–716. [[CrossRef](#)]
3. Meng, Q.S.; Fan, C.; Zeng, W.X.; Yu, K.F. Tests on dynamic mechanical properties of coral reef limestone in Nansha Islands. *Rock Soil Mech.* **2019**, *40*, 183–190. [[CrossRef](#)]
4. Deshpande, V.M.; Madan, S.; Chakraborty, T. Experimental and Numerical Study on Designing Pulse Shapers for Testing Rocks in Large-Diameter SHPB. *J. Mater. Civ. Eng.* **2023**, *35*, 04023012. [[CrossRef](#)]

5. Zheng, Q.Q.; Xu, Y.; Yin, Z.Q.; Wang, F.; Zhang, H.J. Dynamic tensile behaviour under impact loading for rocks damaged by static precompression. *Arch. Civ. Mech. Eng.* **2023**, *23*, 199. [[CrossRef](#)]
6. Sunita, M.; Tanusree, C.; Vasant, M.; Josh, L.; Brady, B. High Strain-Rate Characterization of Deccan Trap Rocks Using SHPB Device. *J. Mater. Civ. Eng.* **2018**, *30*, 04018059. [[CrossRef](#)]
7. Wen, S.; Huang, R.Z.; Zhang, C.S.; Zhao, X.W. Mechanical behavior and failure mechanism of composite layered rocks under dynamic tensile loading. *Int. J. Rock Mech. Min. Sci.* **2023**, *170*, 105533. [[CrossRef](#)]
8. Fakhimi, A.; Azhdari, P.; Kimberley, J. Physical and numerical evaluation of rock strength in Split Hopkinson Pressure Bar testing. *Comput. Geotech.* **2018**, *102*, 1–11. [[CrossRef](#)]
9. Yue, C.J.; Chen, L.; Yuan, J.Y.; Li, Q.Y.; Xu, L.F. A new analytical method for impact splitting strain rate in Brazilian disc test based on SHPB. *Mater. Struct.* **2023**, *56*, 66. [[CrossRef](#)]
10. Demirdag, S.; Tufekci, K.; Kayacan, R.; Yavuz, H.; Altindag, R. Dynamic mechanical behavior of some carbonate rocks. *Int. J. Rock Mech. Min. Sci.* **2010**, *47*, 307–312. [[CrossRef](#)]
11. Ke, Q.R.; Li, C.D.; Yao, W.M.; Fan, Y.B.; Zhan, H.B. Comparative characterization of sandstone microstructure affected by cyclic wetting-drying process. *Int. J. Rock Mech. Min. Sci.* **2023**, *170*, 105486. [[CrossRef](#)]
12. Tan, H.; Li, J.T.; Shi, Z.M.; Wang, M.X.; Wang, J. Damage evolution and failure characteristics of red sandstone with prefabricated crack under coupled dry-wet cycle-fatigue loading. *Int. J. Fatigue* **2023**, *175*, 107751. [[CrossRef](#)]
13. Chai, S.B.; Song, L.; Liu, H.; Abi, E.; Liu, S. Compression characteristics of filled jointed rock under dry-wet cycles. *J. Traffic Transp. Eng.* **2023**, *23*, 142–153. [[CrossRef](#)]
14. Wang, J.K.; Sun, Q.; Xue, S.Z.; Yang, X.Y.; Guo, H. Study on the effect of high-temperature dry-wet cycles on argillaceous sandstone. *Bull. Eng. Geol. Environ.* **2023**, *82*, 318. [[CrossRef](#)]
15. Wei, E.J.; Hu, B.; Li, J.; Zhang, Z.; Ma, L.Y. Study on creep mechanical properties of carbonaceous shale under dry-wet cycle. *Phys. Scr.* **2023**, *98*, 095022. [[CrossRef](#)]
16. Li, Z.G.; Liu, W.; Ye, H.L.; Xu, G.L.; Zhang, Z.W.; Ma, Y. Shear strength damage and degradation model of mica quartz schist under dry-wet cycling [J/OL]. *J. Eng. Geol.* **2023**, 1–7. [[CrossRef](#)]
17. Zhu, J.B.; Fu, Y.Z.; Li, R.; Liao, Z.Y.; Sun, C.; Tang, W.X. Experimental study on mechanical properties of sandstone under coupled dry-wet cycling and dynamic compression. *Chin. J. Rock Mech. Eng.* **2023**, *42*, 3558–3566. [[CrossRef](#)]
18. Liu, X.X.; Li, Y.; Fan, Z.J.; Li, S.N.; Wang, W.W.; Dong, P. Study on energy evolution and failure characteristics of single fracture carbonaceous shale under dry and wet cycling. *Rock Soil Mech.* **2022**, *43*, 1761–1771. [[CrossRef](#)]
19. Wen, T.; Wang, Y.K.; Tang, H.M.; Zhang, J.R.; Hu, M.Y. Damage Evolution and Failure Mechanism of Red-Bed Rock under Drying-Wetting Cycles. *Water* **2023**, *15*, 2684. [[CrossRef](#)]
20. Li, D.Y.; Wang, T.; Cheng, T.J.; Sun, X.L. Static and dynamic tensile failure characteristics of rock based on Ring splitting test. *Trans. Nonferrous Met. Soc. China* **2016**, *26*, 1912–1918. [[CrossRef](#)]
21. Hua, W.; Dong, S.M.; Li, Y.F.; Xu, J.G.; Wang, Q.Y. The influence of cyclic wetting and drying on the fracture toughness of sandstone. *Int. J. Rock Mech. Min. Sci.* **2015**, *78*, 331–335. [[CrossRef](#)]
22. Wu, Q.H.; Zhao, F.J.; Li, X.B.; Wang, S.M.; Wang, B.; Zhou, Z.H. Study on mechanical properties of ring sandstone samples under radial compression. *Rock Soil Mech.* **2018**, *39*, 3969–3975. [[CrossRef](#)]
23. He, Z.L.; Wang, F.; Deng, J.H.; Chen, F.; Li, H.; Li, B. Fracture and energy evolution of rock specimens with a circular hole under multilevel cyclic loading. *Theor. Appl. Fract. Mech.* **2023**, *127*, 103996. [[CrossRef](#)]
24. Li, L.; Luo, L.; Wu, L.Z.; Wang, Q.Z. Dynamic crack propagation and crack arrest of a single crack platform disk with an eccentric circular hole. *Explos. Shock. Waves* **2018**, *38*, 1218–1230.
25. Liu, J.P.; Li, Y.Y.; Xu, S.D.; Xu, S.; Jin, C.Y.; Liu, Z.S. Moment tensor analysis of acoustic emission for cracking mechanisms in rock with a pre-cut circular hole under uniaxial compression. *Eng. Fract. Mech.* **2015**, *135*, 206–218. [[CrossRef](#)]
26. Ulusay, R. *The ISRM Suggested Methods for Rock Characterization, Testing and Monitoring: 2007–2014*; Springer International Publishing: Cham, Switzerland, 2015; pp. 51–68.
27. Chinese Society of Rock Mechanics and Engineering. *Technical Specification for Testing Method of Rock Dynamic Properties; T/CSRME001*; Chinese Society of Rock Mechanics and Engineering: Beijing, China, 2019.
28. *GB/T 50266—2013*; Engineering Rock Mass Test Method Standard. China Planning Press: Beijing, China, 2013.
29. Yuan, P.; Ma, Q.Y. Experimental Study on separated Hopkinson pressure bar in Coal mine sandstone under dry and wet cycle. *Rock Soil Mech.* **2013**, *34*, 2557–2562. [[CrossRef](#)]

**Disclaimer/Publisher's Note:** The statements, opinions and data contained in all publications are solely those of the individual author(s) and contributor(s) and not of MDPI and/or the editor(s). MDPI and/or the editor(s) disclaim responsibility for any injury to person or property resulting from any ideas, methods, instructions or products referred to in the content.